J Neurophysiol 104: 258–270, 2010.
First published May 5, 2010; doi:10.1152/jn.00492.2009.

Cholinergic Modulation of the Resonance Properties of Stellate Cells in Layer II of Medial Entorhinal Cortex

James G. Heys, Lisa M. Giocomo, and Michael E. Hasselmo
Center for Memory and Brain, Program in Neuroscience, and Psychology Department, Boston University, Boston, Massachusetts

Submitted 4 June 2009; accepted in final form 3 May 2010

Heys JG, Giocomo LM, Hasselmo ME. Cholinergic modulation of the resonance properties of stellate cells in layer II of medial entorhinal cortex. *J Neurophysiol* 104: 258–270, 2010. First published May 5, 2010; doi:10.1152/jn.00492.2009. In vitro whole cell patch-clamp recordings of stellate cells in layer II of medial entorhinal cortex show a subthreshold membrane potential resonance in response to a sinusoidal current injection of varying frequency. Physiological recordings from awake behaving animals show that neurons in layer II medial entorhinal cortex, termed "grid cells," fire in a spatially selective manner such that each cell's multiple firing fields form a hexagonal grid. Both the spatial periodicity of the grid fields and the resonance frequency change systematically in neurons along the dorsal to ventral axis of medial entorhinal cortex. Previous work has also shown that grid field spacing and acetylcholine levels change as a function of the novelty to a particular environment. Using in vitro whole cell patch-clamp recordings, our study shows that both resonance frequency and resonance strength vary as a function of cholinergic modulation. Furthermore, our data suggest that these changes in resonance properties are mediated through modulation of h-current and m-current.

INTRODUCTION

A characteristic feature of stellate cells (SCs) in layer II medial entorhinal cortex (mEC) is the existence of 1–5 mV amplitude subthreshold membrane potential oscillations (MPOs) (Alonso and Llinas 1989). Although these unique electrophysiological dynamics were first studied >20 yr ago, more recently it has been shown that stellate cells demonstrate subthreshold membrane potential resonance (Erchova et al. 2004; Hutcheon and Yarom 2000; Lampl and Yaron 1997). Several models have been proposed to explain the generation of MPOs and membrane potential resonance (Dickson et al. 2000; Dudman and Nolan 2009; Erchova et al. 2004; Fransen et al. 2004; Haas et al. 2002; Nolan et al. 2007; White et al. 1998, 2000). The circuit used to describe the stellate cell membrane potential response is well modeled by a resistive-capacitive-inductive circuit. The inductive component produces a decreasing voltage response to injected currents of decreasing frequency and endows such neurons with band-pass filtering capabilities. Previous research on SCs has shown that the inductive component that produces such a voltage response and endows the cell with membrane potential resonance is the h-current (I_h) (Haas et al. 2002; Nolan et al. 2007).

The relationship between the subthreshold resonance and firing behavior of mEC SCs has been analyzed to show that resonant neurons display spike clustering with constant intracluster interspike intervals (ISIs) as a function of injected current, resulting in a multimodal ISI probability density function (Engel et al. 2008). This feature is absent in the spike train of nonresonant cells, which show a monotonically decreasing ISI as a function of injected depolarizing current.

In recordings from behaving rats, cells in mEC termed "grid cells" fire in a spatially selective pattern such that each cell's multiple firing fields are arranged in a nearly symmetric hexagonal grid (Barry et al. 2007; Fyhn et al. 2004; Hafting et al. 2005; Moser and Moser 2008; Sargolini et al. 2006). Subthreshold membrane potential resonance shows a relation to the firing behavior of these cells. The subthreshold MPO and resonant frequency differ from higher to lower frequencies in SCs along the dorsal to ventral axis of mEC (Giocomo et al. 2007), which correlates with a systematic increase in grid field spacing along this same axis (Hafting et al. 2005; Sargolini et al. 2006). Subsequent experimental work has also shown that the h-current time constant increases along the dorsal to ventral axis of mEC (Giocomo and Hasselmo 2008), and biophysical modeling has shown that this change in the time constant can account for the difference in both subthreshold MPO and resonant frequency shown in dorsal and ventral SCs (Heys et al. 2008).

Limited research has been conducted to show how subthreshold membrane potential resonance and spiking behavior might be regulated as a function of neuromodulation (Klink and Alonso 1997b). Previous studies conducted by Pian et al. (2006) showed that, in xenopus oocytes expressing muscarinic M1 receptors and hyperpolarization-activated cyclic nucleotide-regulated (HCN) channels, activation of muscarinic acetylcholine receptors causes a twofold slowing of the time constant of the h-current comprised of HCN2 homomers (Pian et al. 2006, 2007). These data suggest that modulatory influences could alter the resonance properties of entorhinal neurons and thereby alter the response properties of entorhinal grid cells. Consistent with this, data show that grid field spacing increases when an animal encounters a novel environment (Barry et al. 2009). These changes could be induced by modulation of acetylcholine (ACh) levels, which change in response to environment novelty and during behavioral contexts such cue detection (Acquas et al. 1996; Parikh et al. 2007).

We asked the question of how muscarinic acetylcholine receptor (mAChR) activation can modulate resonance properties in SCs in mEC. To answer this question, we used a combination of in vitro whole cell patch-clamp recordings of SCs in mEC and biophysical modeling. Using the standard impedance amplitude profile (ZAP) protocol, which consists of injecting a sinusoidal current of constant amplitude and linearly increasing frequency, we were able to measure the injected current frequency that gave the largest amplitude

Address for reprint requests and other correspondence: J. G. Heys, Program in Neuroscience, Boston Univ., 2 Cummington St., Boston, MA 02215 (E-mail: jimheys@bu.edu).

voltage response (Hutcheon et al. 1996). This largest amplitude response, termed the resonant frequency, was measured before and after application of the muscarinic agonist carbachol. In this way, it was possible to assess the effects of mAChR-dependent modulation of resonance properties. Furthermore, through the use of biophysical modeling and pharmacological manipulations, it was possible to show how these changes were mediated by modulation of h-current and m-current (I_m).

METHODS

Slice preparation

All electrophysiological data presented in this study were collected from male and female Long Evans rats, aged 17–23 days old (Charles River Laboratories, Wilmington, MA). The Institutional Animal Care and Use Committee at Boston University approved all experimental techniques. After deep anesthetization with Isoflurane (Abbott Laboratories, North Chicago, IL), the animal was decapitated, and the brain was rapidly removed under 4°C artificial cerebrospinal fluid (ACSF; concentrations in mM: 126.0 NaCl, 3 KCl, 2 $MgSO_4$, 10.0 dextrose, 26.0 $NaHCO_3$, 1.25 NaH_2PO_4, and 2 $CaCl_2$), oxygenated by bubbling 95% O_2-5% CO_2 through the solution.

Whole cell patch-clamp recordings were taken from 400 μm slices, and the depth of each slice was measured using the same protocol as Giocomo et al. (2007). Accordingly, the brain was cut into quarters along the corpus callosum and 4 mm from the rostral surface of the brain (−4 mm Bregma). Previous research has shown that electrophysiological recordings are not affected by the order of the slicing procedure (Giocomo et al. 2007). Therefore all recordings were made from slices cut from the dorsal to the ventral surface of mEC.

Once the slicing procedure was completed, the slices were incubated for 30 min in a heat bath at 31°C and then at room temperature for 30 min. All recording experiments were performed at the physiological temperature of 37°C. Slices were imaged using an upright microscope (Axioskop, Zeiss, Thornwood, NY) equipped with a ×40 water-immersion objective lens (Zeiss). Whole cell patch-clamp recordings were conducted using 4–8 MΩ pipette (10 cm) borosilicate glass capillary tubes (Sutter Instruments), which were pulled using a Sutter Instruments model P-87 pipette puller. The pipettes were loaded with a solution containing (in mM) 120 K-gluconate, 10 HEPES, 0.2 EGTA, 20 KCl, 2 MgCl, 7 diTrisPhCr, 4 Na_2ATP, and 0.3 TrisGTP (pH adjusted to 7.3 with KOH). The intracellular solution contained 0.1% biocytin for morphological identification and staining of the cells. Individual slices were placed in a Warner Instruments Series 20 Chamber. The chamber was filled with oxygenated ACSF, and the solution was continuously exchanged. The seal between the cellular membrane and pipette was ruptured using negative pressure once the seal was >1 GΩ. In current-clamp mode, the voltage was amplified using a Multiclamp 700B (Molecular Devices, Sunnyvale, CA). Capacitance neutralization and bridge balance were applied accordingly. Current-clamp data were low-pass filtered at 10 kHz. Data were digitized with a Digidata 1320 at a sampling frequency of 20 kHz (50 μs). Signals were acquired using a Pentium-based computer running Clampex 10.0 software (Axon Instruments). For all solutions, the hypothetical liquid junction potential was estimated between 5 and 6 mV using the technique of Neher (1992) and Dickson et al. (2000). Membrane potential values reported here do not contain this correction. After recording, slices were placed in a 4% paraformaldehyde solution.

All 58 SCs were identified by the presence of subthreshold membrane potential oscillations and a large sag potential. Twenty-five of these cells were also stained by biocytin and identified on the basis of their morphology (Klink and Alonso 1997a). Staining also confirmed the location of SCs in layer II of the mEC. SCs were defined as being located in the dorsal mEC if they were positioned 3.8–4.9 mm ventral to Bregma and defined as being located in the ventral mEC if positioned 5.0–7.0 mm ventral to Bregma. Coordinates were based on Paxinos and Watson (1998). All cells used were held for ≥30 min, had an input resistance of ≥35 MΩ, had an action potential height of ≥50 mV from threshold to peak, and had a resting potential of ≤ −50 mV. Data are expressed as mean ± SE. The statistical analysis was performed using a two-tailed Student's *t*-test (MATLAB). The linear regression analysis was done using Microsoft Excel statistical analysis software.

Solutions

For all experimental solutions, 2 mM kynurenic acid and 100 μM picrotoxin were added to block synaptic transmission (Sigma Aldrich, St. Louis, MO). To activate acetylcholine receptors, 10 μM carbachol solution was used for current-clamp protocols. To block activation of mAChRs, a 1 μM concentration of atropine was used. To block the m-current, 10 μM XE991 (Tocris Cookson) was added to the solution. To block the h-current, a 10 μM concentration of ZD7288 was used.

Data analysis

MEMBRANE POTENTIAL RESONANCE PROFILE. To obtain the impedance amplitude profile, cells were stimulated with a 20 s, constant amplitude sinusoidal current injection, $I(t)$, which increased linearly from 0 to 20 Hz over time (Erchova et al. 2004; Gimbarzevsky et al. 1984; Hutcheon and Yarom 2000). The sinusoidal current was generated in MATLAB by the chirp function. To maintain each cell's resting potential across control and experimental conditions, a steady depolarizing or hyperpolarizing current was injected. The resulting voltage response, $V(t)$, was measured, and the frequency-dependent impedance profile, $Z(f)$, was calculated by taking the ratio of the fast Fourier transform (FFT) of the voltage response divided by the FFT of the injected sinusoidal current

$$Z(f) = \frac{FFT[V(f)]}{FFT[I(f)]}$$

The resonance frequency, f_{res}, was defined as the frequency of injected current that maximized $Z(f)$. Resonance strength, Q, was defined as

$$Q = \frac{Z(f_{res})}{Z(f_{min})}$$

where f_{min} was set to 0 Hz by fitting the impedance profile with a fourth-order polynomial and extrapolating to find the impedance value at 0 Hz. f_{res} and Q were measured five times in each cell under each experimental condition, and the resonant frequency and resonant strength were recorded as the average across the five trials in each condition.

SAG ANALYSIS. Because of the rectifying nature of I_h, its time course and relative magnitude across experimental conditions could be measured by applying a hyperpolarizing current step and analyzing the resulting "sag" in the membrane potential (Alonso and Klink 1993). The time course and amplitude of this hyperpolarizing membrane potential rectification was measured from voltage traces that had steady-state potentials of −76 to −70 mV. Cells were held in current clamp at −65 mV, and 3 s long hyperpolarizing current injections were given at a range of amplitudes. MATLAB's NonlinearLeastSquares method was used in combination with MATLAB's function exp2 to analyze the time constant of the sag. Current-clamp data were fitted with the following double exponential function

$$F = A_1 \exp^{(-t/\tau_1)} + A_2 \exp^{(-t/\tau_2)}$$

where A_1 and A_2 are the amplitude of the fast (τ_1) and slow (τ_2) component of the sag, respectively. Sag potentials were used for the fitting, starting from the trough of the sag response plus 7 ms (to pass

the trough) and ending before the end of the current pulse (−4 ms, to avoid any stimulation artifact). Time constants (τ_1 and τ_2) were used in the subsequent analysis, and analysis was performed only on traces with an endpoint voltage of between −76.0 and −70.0 mV.

Biophysical model

Using the NEURON simulation software, a model of an EC SC was constructed with a single compartment with dimensions listed below. Similar to previous models (Dickson et al. 2000; Fransen et al. 2004), we used a simplified model containing currents previously proposed to underlie membrane potential oscillations: the I_h and persistent sodium current (I_{NaP}) currents. The m-current was taken from a model of a CA1 pyramidal neuron used in Migliore 1995. These currents were modeled using the Hodgkin-Huxley formalism in an equivalent circuit representation of membrane potential dynamics as follows

$$C_m\frac{dV}{dt} = \bar{g}_{H(fast)}\, n(V_m - E_H) + \bar{g}_{H(slow)}\, k(V_m - E_H) + \bar{g}_{NaP}\, mh(V_m - E_{NaP}) + \bar{g}_M s(V_m - E_K) + \bar{g}_{leak}(V_m - E_{leak}) + I_{app}$$

In this equation, V_m indicates membrane potential and C_m is membrane capacitance. For different components of membrane conductance, $\bar{g}_x$ indicates the maximum conductance and E_x indicates the reversal potential. I_{app} represents injected current. The variables n, k, s, m, and h indicate activation or inactivation kinetics for voltage-sensitive components with the standard structure

$$\frac{dx}{dt} = \frac{(x_{inf} - x)}{\tau}$$

The kinetics of I_{NaP} were modeled according to Fransen et al. (2004) for I_{NaP} activation and Magistretti and Alonso (1999) for I_{NaP} inactivation. The MATLAB curve fitting tool was used to fit the I_h time constants and the steady-state activation functions obtained in experimental voltage-clamp data from SCs presented in Giocomo and Hasselmo 2008. The gating variables for each active conductance were modeled as follows

I_h (fast):
Activation:

$$\tau_n(V) = \frac{38.6}{\exp\left[(V_m + 109.2)/(-28.2)\right] + \exp\left[(V_m + 2.8)/21.3\right]}$$

$$n_{inf}(V) = \frac{1}{1 + \exp\left[(V_m + 68.08)/7.14\right]}$$

I_h (slow):
Activation:

$$\tau_k(V) = \frac{330.0}{\exp\left[(V_m + 38.2)/(0.72)\right] + \exp\left[(V_m + 112.0)/(-51.9)\right]}$$

$$k_{inf} = \frac{1}{1 + \exp\left[(V_m + 68.08)/7.14\right]}$$

I_{Nap}:
Activation:

$$\alpha_m(V) = \frac{91 \times 10^{-3}\,(V - 38)}{1 - \exp\left[-\left(\frac{V + 38}{5}\right)\right]}$$

$$\beta_m(V) = \frac{-62 \times 10^{-3}(V + 38)}{1 - \exp\left(\frac{V + 38}{5}\right)}$$

$$\tau_m = \frac{1}{\alpha_m + \beta_m}$$

$$m_{inf} = \frac{1}{1 + \exp\left[-\left(\frac{V + 48.7}{4.4}\right)\right]}$$

Inactivation:

$$\alpha_h(V) = \frac{10^{-5}(-0.288V - 4.9)}{1 - \exp\left(\frac{V + 17.01}{4.63}\right)}$$

$$\beta_h(V) = \frac{10^{-3}(6.94 \times 10^{-3}V - 0.447)}{1 - \exp\left[-\left(\frac{V + 64.41}{2.63}\right)\right]}$$

$$\tau_h = \frac{1}{\alpha_h + \beta_h}$$

$$h_{inf} = \frac{1}{1 + \exp\left(\frac{V + 48.8}{9.98}\right)}$$

I_m:
Activation:

$$\alpha_s(V) = \exp\left[-24.443 \times 10^3(V + 55)\right]$$

$$\beta_s(V) = \exp\left[-19.5546 \times 10^3(V + 55)\right]$$

$$\tau_s = \frac{\beta_s}{5^{3/2} \times 0.0002(1 + \alpha_s)}$$

$$s_{inf} = \frac{1}{1 + \alpha_s}$$

Passive membrane parameters:

$$C_m = 1.0\ \mu F/cm^2$$

$$E_{leak} = -90\ mV$$

The maximum conductance and reversal potentials were as follows: $\bar{g}_{H(fast)} = 0.00013$ (S/cm^2); $\bar{g}_{h(slow)} = 0.000079$ (S/cm^2); $\bar{g}_{NaP} = 0.00006$ (S/cm^2); $\bar{g}_{leak} = 0.00008$ (S/cm^2), $\bar{g}_M = 0.00007$ (S/cm^2); $E_h = -20$ mV; $E_{NaP} = 87$ mV. The maximum conductance values were chosen to give physiologically relevant membrane resistance, sag response, resonance frequency, resonance strength, MPO frequency, and MPO amplitude.

In the simulations, the morphology of the entorhinal cortical layer II SC was reduced to a single cylindrical compartment. The somatic compartment had a diameter of 30 μm and a length of 30 μm. The temperature of the model cell was set to 37°C.

Using the NEURON simulation software, the Crank-Nicolson method was applied to obtain numerical solutions of the differential equations. The time step for the numerical integration was 0.025 ms.

RESULTS

The ZAP response is a useful way to characterize the electrophysiological profile of mEC layer II SCs. In accordance with results from coexpression of HCN1, HCN2, and mAChR in *Xenopus* oocytes (Pian et al. 2006, 2007), we predicted that cholinergic activation would modulate the subthreshold membrane potential resonance in SCs. To test this prediction, the ZAP response of SCs was compared in control solution and after 10 min bath application of 10 μM carbachol,

which is a nonselective AChR agonist. The input resistance, averaged across all cells, was 52.7 ± 3.6 MΩ ($n = 23$) in control and increased to 67.8 ± 4.1 MΩ ($n = 23$) after the 10 min bath application of carbachol. The modulation of the ZAP response is twofold and can be easily discerned by inspection of recordings from individual SCs (Fig. 1*A*). First, in 21 of 23 cells, the resonance frequency was reduced on activation of mAChRs (Fig. 1*B, left*). Second, we note that resonance strength was also reduced on activation of mAChRs in 22 of 23 cells (Fig. 1*B, right*). As shown in Fig. 1*B* (*left*), the averages across all SCs show that in control, resonance frequency was 6.71 ± 0.35 Hz, and in the carbachol condition, resonance frequency was 5.01 ± 0.31 Hz ($P < 0.01$, $n = 23$). Similarly, the averages across the cell population showed that resonance strength was reduced from 1.68 ± 0.04 in control to 1.44 ± 0.04 ($P < 0.01$, $n = 23$) in carbachol (Fig. 1*B, right*). Both of these effects are captured in the frequency domain by plotting the average impedance profile in control and carbachol conditions (Fig. 1*C*).

The ZAP response in 10 μM carbachol was recorded from an additional set of five cells using smaller-amplitude ZAPs to control for the possibility of differential channel activation at the positive and negative peaks of the ZAP response. Consistent with the original result, the resonance frequency, using the smaller ZAP protocol, decreased from 6.4 ± 0.3Hz in control to 4.6 ± 0.3Hz in carbachol ($P < 0.01$, $n = 5$). Similarly, the resonance strength decreased from 1.68 ± 0.02 in control to 1.47 ± 0.08 in carbachol ($P < 0.05$, $n = 5$).

We performed control experiments and determined that carbachol was acting through muscarinic acetylcholine receptors. To this end, the ZAP response was recorded in control with 1 μM atropine, which is a competitive mAChR antagonist, and again after 10 min bath application of 1 μM atropine with 10 μM carbachol. Results from ZAP protocols are shown in a recording from an individual SC, and there are no significant differences in resonance frequency or resonance strength across the two conditions (Fig. 2*A*). A plot of the impedance profile across all cells in the control experiment showed no significant differences between the atropine and atropine with carbachol conditions (Fig. 2*C*). Averages across all SCs ($n = 8$) showed the change in resonance frequency was −0.07 ± 0.01 Hz when changing from the atropine to atropine with carbachol, which was not statistically different from mean zero. In contrast, the change in resonance frequency from the control to the carbachol condition previously shown in Fig. 1*B* was −1.70 ± 0.25 Hz. As shown in Fig. 2*E* (*left*), the change in resonance when adding carbachol alone was significantly greater than the change in resonance when adding carbachol in atropine ($P < 0.01$, $n = 8$ for atropine to atropine with carbachol condition and $n = 23$ for control to carbachol condition). The difference between the value of the resonance frequency in carbachol alone (5.01 ± 0.31 Hz, $n = 23$; Fig. 1) and the resonance frequency in carbachol and atropine (6.80 ± 0.53 Hz, $n = 8$; Fig. 2, *A, C*, and *E*) was statistically significant ($P < 0.05$). The resonance strength also did not change significantly after carbachol was applied to a control solution of atropine (Fig. 2*E, right*). The change in resonance strength from the atropine solution to atropine with carbachol was 0.013 ± 0.018, and the change in resonance strength from control to carbachol shown previously in Fig. 2*B* is −0.238 ± 0.038 ($P < 0.01$, $n = 8$ for atropine to atropine with carbachol condition and $n = 23$ for control to carbachol condition). The difference between absolute value of the resonance strength in carbachol alone (1.44 ± 0.04, $n = 23$; Fig. 1) and resonance strength in carbachol plus atropine (1.71 ± 0.06, $n = 8$) was statistically significant ($P < 0.01$).

A second control study was performed to ensure the observed change in membrane potential resonance could not be explained by channel rundown induced by whole cell patch-clamp washout. Here resonance properties were initially measured in control solution and again in control solution after a 15 min wait period. Recording from individual SCs clearly showed there were no differences in resonance frequency or resonance strength (Fig. 2*B*). A plot of the impedance profile across all cells in the control experiment showed no significant differences between the control and time control conditions (Fig. 2*D*). Neither the change in resonance frequency nor the change in resonance strength from the control to the time control conditions was statistically different from mean zero. As stated previously, the population average of the change in resonance frequency was −1.70 ± 0.25 Hz between control versus carbachol conditions. As shown in Fig. 2*F*, this was significantly different from the change in resonance frequency from control to the time control condition (−0.38 ± 0.16 Hz; $P < 0.01$, $n = 23$ in carbachol condition and $n = 7$ in the time control condition). The difference between value of the resonance frequency in carbachol (5.01 ± 0.31 Hz, $n = 23$) and resonance frequency after 15 min in the time control condition (6.41 ± 0.55 Hz, $n = 7$) was statistically significant ($P < 0.05$). The change in resonance strength from control to carbachol was −0.238 ± 0.038, which was significantly greater than the change from control to time control (−0.013 ± 0.077; $P < 0.01$, $n = 23$ and $n = 7$). Similarly, the value of the resonance strength in carbachol (1.44 ± 0.04, $n = 23$) was significantly different from that of the resonance strength after the 15 min time control (1.63 ± 0.06, $n = 7$; $P < 0.05$).

Results from Pian et al. (2006) showed that h-current produced by exclusively HCN1 or HCN2 homomers can be differentially modulated through activation of receptors that interact with the phospholipase C pathway, which includes mAChRs. Furthermore, a difference in baseline resonance frequency along the dorsal to ventral axis of mEC could be explained by differential HCN subunit composition along the dorsal to ventral axis (Giocomo and Hasselmo 2008, 2009). Taken together, these two pieces of information could predict a differential change in cholinergic modulation of h-current–dependent resonance properties along the dorsal to ventral axis of mEC. This hypothesis was tested by measuring the percentage change in resonance frequency across control to the carbachol condition in SCs along this axis (Fig. 3*A*). The slope of the linear fit to these data was statistically different from zero ($P < 0.01$). By partitioning SC recordings into a dorsal subdivision (3.8–4.9 mm) and a ventral subdivision (5.0–6.2 mm), the average change in resonance frequency after application of carbachol was compared across regions. The population averages in control solution among dorsal SCs were shown to be 7.28 ± 0.35 Hz ($n = 15$) and ventral SCs were shown to be 5.64 ± 0.62 Hz ($n = 8$; $P < 0.05$; Fig. 3*B*). The population averages in carbachol solution among dorsal SCs were shown to be 5.71 ± 0.28 ($n = 15$) Hz and ventral SCs were shown to be 3.68 ± 0.45 Hz ($n = 8$; $P < 0.01$; Fig. 3*B*). Similar to the results shown in Fig. 1, when each partitioned

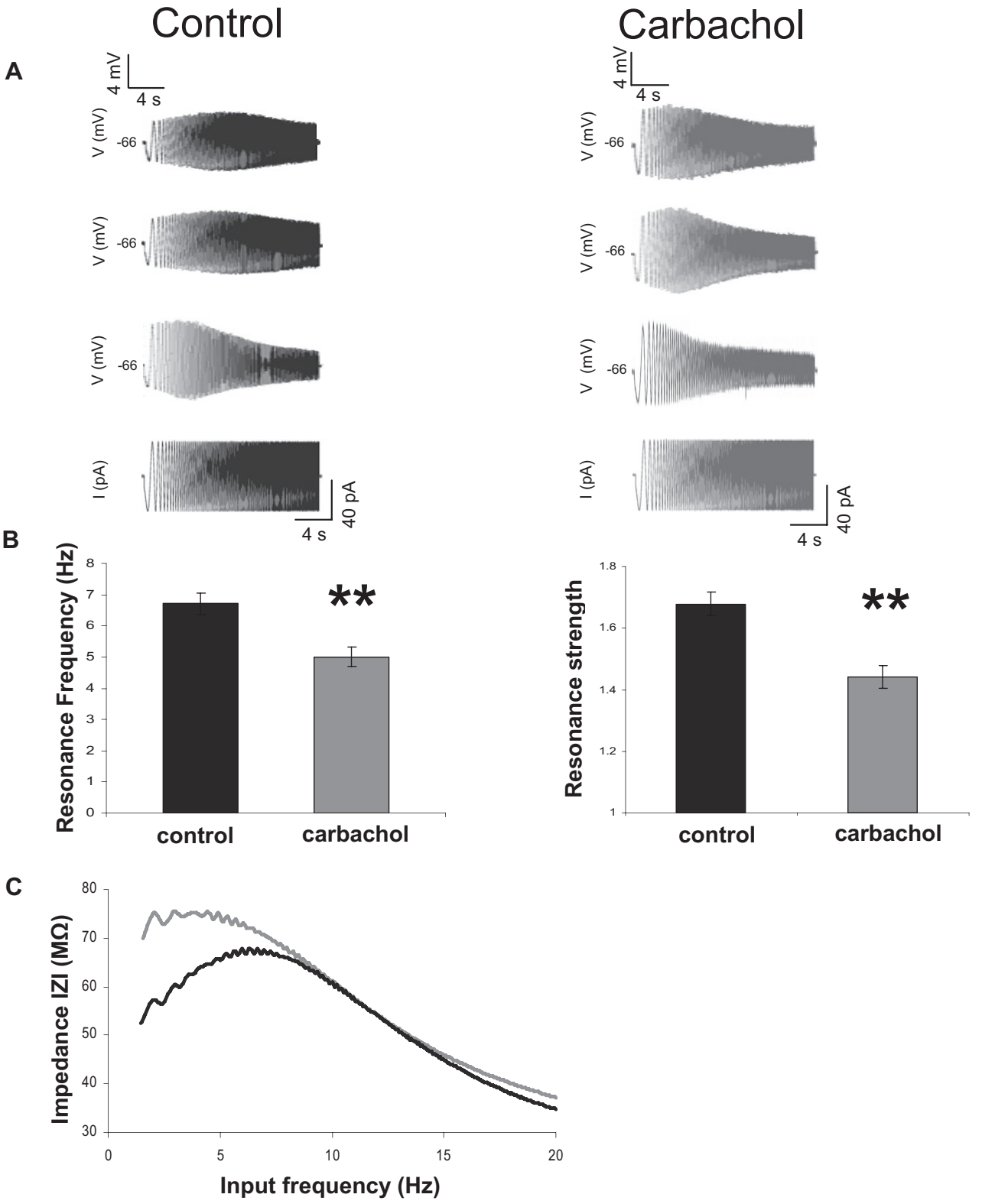

FIG. 1. Application of carbachol significantly reduces resonance frequency and resonance strength of medial entorhinal cortex (mEC) stellate cells (SCs). *A*: representative examples of standard impedance amplitude profile (ZAP) response of stellate cells in control (black) and in 10 μM carbachol (gray). In both conditions, cells were held at −66 mV and injected with a 20 s ZAP stimulus with 65 pA amplitude, shown on the *bottom* of *A*. *B*: SC population averages of resonance frequency (Hz) and resonance strength in control and carbachol conditions. *C*: average impedance profile in control (black) and carbachol (gray) across all cells.

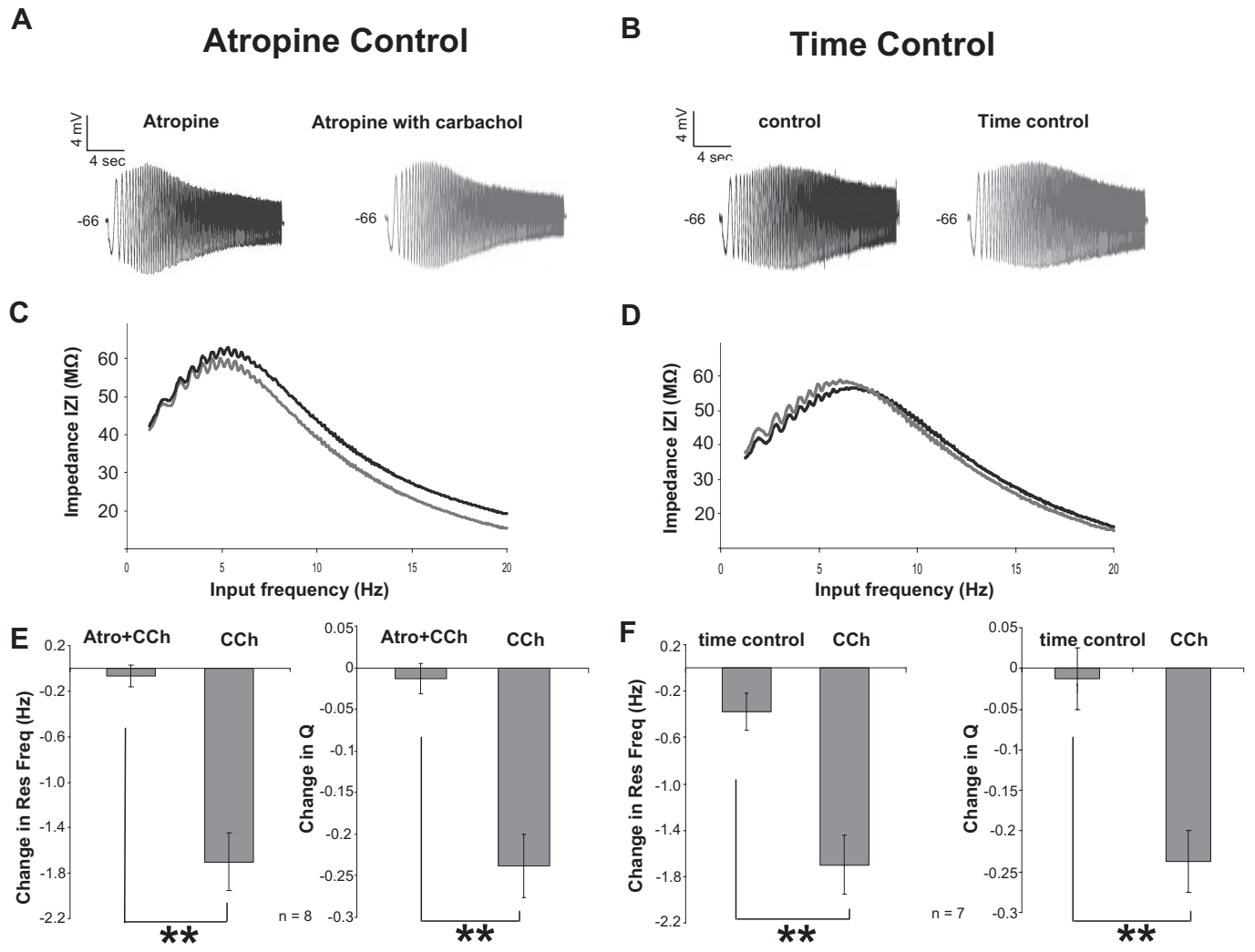

FIG. 2. Control experiments show that the change in resonance properties result from activation of muscarinic acetylcholine receptors and are not caused by whole cell patch-clamp–induced washout and channel rundown. *A* and *B*: examples of the voltage response of SCs generated from injection of a ZAP stimulus of 65 pA amplitude. *A*: the voltage response was measured in 1 μM atropine (black) and after 10 min bath application of 10 μM carbachol with 1 μM atropine (gray). *B*: the voltage response was measured in control (black) and in time control condition (gray), which consisted of waiting 15 min after the last control ZAP stimulus was injected. *C*: the frequency dependent impedance profile was averaged across all cells in atropine (black) and in atropine with carbachol (gray). *D*: the impedance profile was measured in control condition (black) and in time control condition (gray). *E*: average change in resonance frequency (Hz) and resonance strength across all atropine with carbachol (Atro + CCh) control experiments is contrasted with the change in resonance frequency after application of carbachol (CCh), as presented in Fig. 1. *F*: average change in resonance frequency (Hz) and resonance strength across all time control experiments is contrasted with the change in resonance frequency after application of carbachol (CCh; from Fig. 1).

dorsal and ventral group was compared across the control and carbachol conditions, they both showed a statistically significant decrease in resonance frequency from the control to the carbachol condition (Fig. 3*B*).

Using a biophysical, conductance-based model of mEC SCs, we sought to determine how changes in channel physiology could mediate the observed changes in resonance frequency and resonance strength. Previous experimental work in slice preparations and experimental work using heterologous expression of H-channels suggested the effects of membrane potential resonance could be the result of cholinergic modulation of h-current kinetics and/or channel open probability (Hu et al. 2002; Pian et al. 2006, 2007). Furthermore, as documented previously and shown in this study, application of carbachol increases membrane resistance, which indicates the blocking of passive leak conductances (Cole and Nicoll 1984). Finally, we were interested in testing the possible influence of m-current blockage because this current has been shown to contribute to resonance in CA1 pyramidal neurons and is blocked on application of carbachol (Hu et al. 2002).

To assess membrane potential resonance in the model cell, a simulated sinusoidal current, described by the same function as the ZAP used in experimental paradigm, was injected into the model cell, and the resulting resonance properties were calculated. The results show that changes in leak conductance have little effect on the resonance frequency (Fig. 4, *A* and *C*, *left*). This result is in accordance with data on membrane potential oscillation frequency from Fernandez and White (2008), where the impedance profile was measured in mEC SCs in control and with added leak conductance using dynamic clamp. In contrast, the modulation of leak conductance had a dramatic

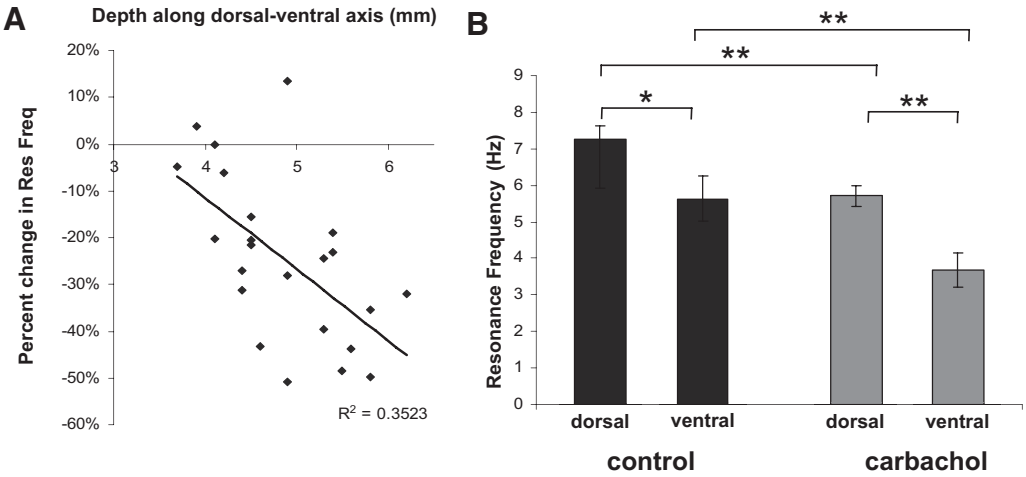

FIG. 3. Stellate cells across the dorsal to ventral axis of mEC show differential changes in resonance frequency as a function of mAChR activation. *A*: SCs in ventral mEC show a larger percentage decrease in resonance frequency on application of carbachol. *B*: resonance frequency is lower in control condition SCs in ventral mEC (5.64 ± 0.62 Hz, $n = 8$) compared with SCs in dorsal mEC (7.28 ± 0.35 Hz, $n = 15$; $P < 0.05$). Resonance frequency measured in carbachol is lower in SCs in ventral mEC (3.68 ± 0.45 Hz, $n = 8$) compared with SCs in dorsal mEC (5.71 ± 0.28 Hz, $n = 15$; $P < 0.01$). The decreases shown in resonance frequency in ventral SCs from the control to the carbachol condition and in dorsal SCs from the control to the carbachol condition are both statistically significant ($P < 0.01$).

effect on resonance strength in the model (Fig. 4, *A* and *C, right*). The carbachol-induced increase in membrane resistance indicated a decrease in the leak conductance, and the simulation results showed this change would have a positive effect on resonance strength, which is contradictory to the experimental results showing a carbachol-induced decrease in resonance strength. Taken together, the lack of effect on resonance frequency in the model and the opposite effect on resonance strength in the model suggest a change in leak conductance does not account for the experimental results about carbachol effects on resonance.

Although there are multiple lines of evidence pointing toward a role for cholinergic modulation of m-current–dependent membrane potential resonance in SCs, experimental evidence has not supported this notion (Yoshida and Alonso 2007). However, the results from the study of Yoshida and Alonso were generated from recordings at 30°C, and the low membrane potential oscillation frequencies measured at this temperature closely match resonance frequencies measured in CA1 pyramidal at these same temperatures (Hu et al. 2002). At higher temperatures, Hu and colleagues showed a significant increase in resonance frequency, and at these higher physiological temperatures, an influence of m-current on membrane potential resonance may become more apparent. To test the potential impact of m-current, the maximum conductance of the m-current was modulated in the model, and the resulting resonance properties were measured. Because the m-current activation occurs at more depolarized potentials relative to other currents active at rest, such as h-current, we simulated results at varying resting potentials. Similar to the results from Hu et al. (2002) in CA1 pyramidal neurons, our simulation results predicted a significant influence of m-current at −58 mV (Fig. 4*A*) and almost no impact at −68 mV (Fig. 4*C*). At more depolarized resting potentials, a carbachol-induced decrease in m-current may in fact contribute to physiological changes described in the Fig. 1.

Finally, we examined the role of the h-current on membrane potential resonance. The results from simulations showed that the maximum conductance of the h-current is positively related to resonance frequency and resonance strength (Fig. 4, *A* and *C*). Similarly, an increase in h-current time constant shifts both resonance frequency and resonance strength to lower values (Fig. 4*E*). Using measurements of h-current steady-state activation and h-current kinetics from voltage-clamp recordings of mEC SCs and using results from Pian and colleagues showing a 1.5- to 2-fold slowing of h-current time constant on activation of mAChRs (from channel expressed in *Xenopus* oocytes), our simulation results showed that similar changes in time constants shift resonance frequency and resonance strength to values that are consistent with experimental results (Fig. 4*E*).

To test the model predictions that cholinergic modulation slows the h-current time constant and changes the h-current maximum amplitude, we used current-clamp recordings of SCs to test the voltage response to DC hyperpolarizing current injections in control and carbachol conditions (Fig. 5*A*). Here the rectification from hyperpolarizing steps or sag clearly decreases in amplitude from 3.82 ± 0.17 to 2.53 ± 0.2 mV ($P < 0.01$, $n = 24$) after activation of mAChRs (Fig. 5*B, right*). The time course of this sag response was fit to a dual exponential, and time constants of this fit showed a significant increase from 22 ± 1 to 29 ± 2 ms ($P < 0.01$, $n = 24$) in the carbachol condition (Fig. 5*B, left*).

Because application of carbachol has been shown to increase input resistance, it could be argued that the changes seen in the sag potential are mediated through changes in leak conductance. However, a decrease in leak conductance should increase the relative contribution of the h-current and therefore increase the sag amplitude, which does not fit with the experimental data. Using this argument, it seems most plausible that changes in the sag amplitude are caused by decreases in the h-current maximum conductance. Part of the change seen in the sag time course could, however, be caused by a carbachol-induced decrease in the leak conductance, because this would increase the membrane time constant and slow the sag time course. Although a decrease in the h-current time constant would also fit these data and would be predicted from the

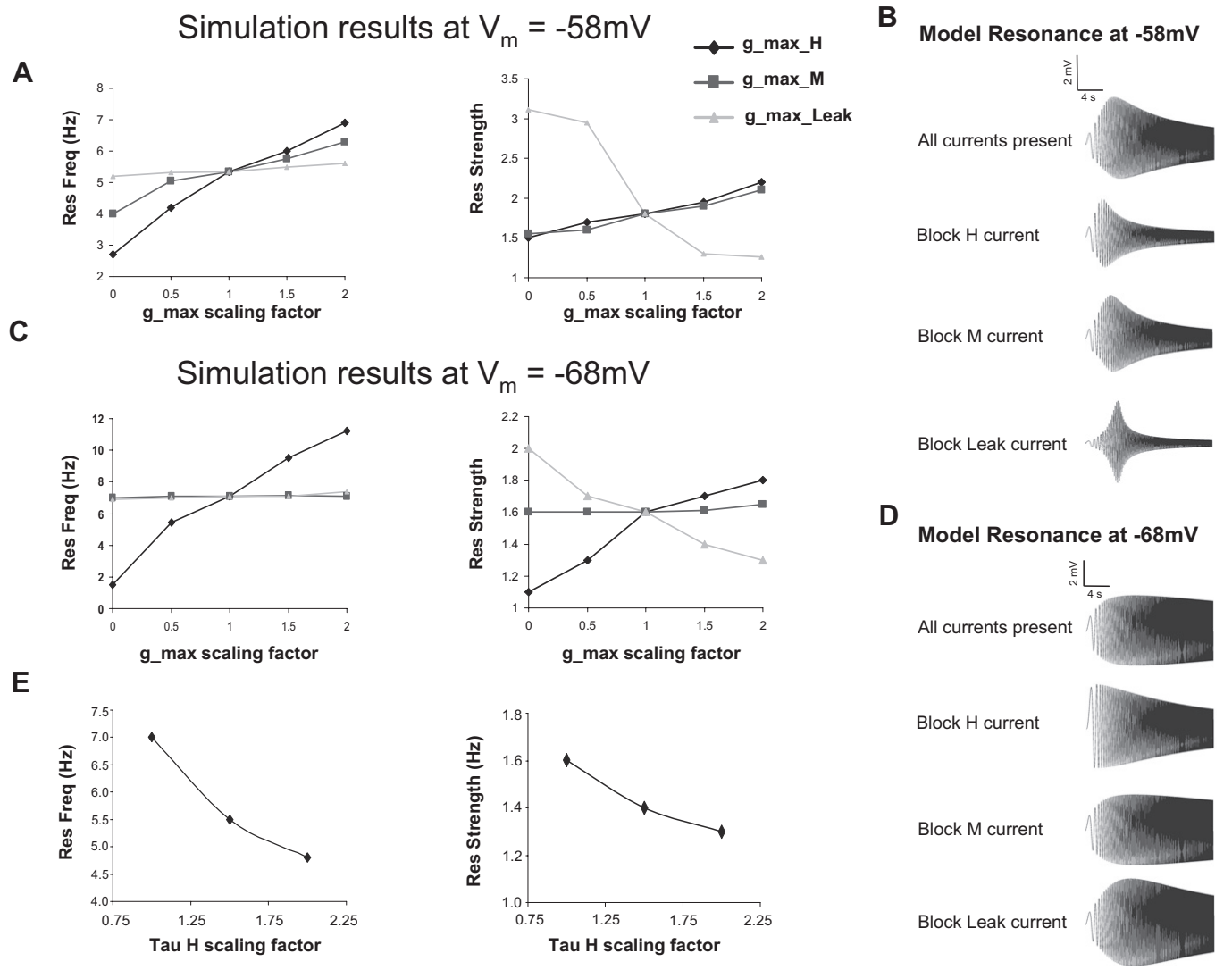

FIG. 4. Simulation results from a biophysical conductance–based model predicts the channel physiology that could mediate the muscarinic acetylcholine receptor (mAChR)-dependent changes in resonance frequency and resonance strength. *A*: resonance properties were measured as a function of the maximum conductance values of the h-current (diamond), m-current (square), and leak current (triangle). At a holding potential of −58 mV, the resonance frequency is shown on the *left* and resonance strength is shown on the *right*. *B*: individual simulations of ZAP protocols are shown at −58 mV in control, h-current block, m-current block, and leak-current block from *top* to *bottom*. *C*: at a holding potential of −68 mV, the resonance frequency is shown on the *left* and resonance strength is shown on the *right*, with the same colors for manipulations of currents in *A*. *D*: individual simulations of ZAP protocols are shown at −68 mV in control, h-current block, m-current block, and leak-current block from *top* to *bottom*. *E*: resonance frequency (*left*) and resonance strength (*right*) were measured as a function of the h-current time constant. The h-current time constant was scaled by factors of 0.5, 1, and 2.

heterologous studies by Pian et al. (2007), we cannot rule out the possibility that some of the changes are caused by a decrease in passive leak conductance.

To further assess the role of the h-current as a mechanism to mediate the cholinergic modulation of the resonance frequency and resonance strength, we ran the ZAP protocol using 10 μM ZD7288, which is a selective h-current blocker. As shown in Fig. 6*A*, the application of ZD7288 decreased the resonance frequency and resonance strength to values close to theoretical minimums (Fig. 6*A*). The application of ZD7288 reduced the resonance frequency from 6.05 ± 0.66 Hz in control to 1.52 ± 0.13 Hz in ZD7288 ($P < 0.01$, $n = 6$; Fig. 6*B, left*). Similarly, the resonance strength was reduced from 1.54 ± 0.07 in control to 1.19 ± 0.06 in ZD7288 ($P < 0.01$, $n = 6$; Fig. 6*B*, *right*). Subsequent application of carbachol did not show any significant effect on either the resonance frequency or the resonance strength when used after the 10 min bath application of ZD7288 (Fig. 6*B*).

To control for the possibility that changes in the sag profile were the result of cholinergic modulation of a current other than the H-current, the voltage response was measured in response to hyperpolarizing current steps in the presence of 10 μM ZD7288 and after a 20 min bath application of 10 μM carbachol with ZD7288. The results shown in Fig. 6*C* demonstrate that ZD7288 completely abolishes the sag response and subsequent application of carbachol has no effect on the voltage response. As shown in Fig. 6*D* (*left*), the sag amplitude in ZD7288 was 0.084 ± 0.034 mV in ZD 7288, and the sag amplitude did not change after application of carbachol (gray, solid; 0.088 ± 0.12 mV; $P = 0.87$, $n = 6$). Furthermore, as shown in Fig. 6*D* (*right*), the change in the sag amplitude from control ACSF to carbachol is significantly different from the

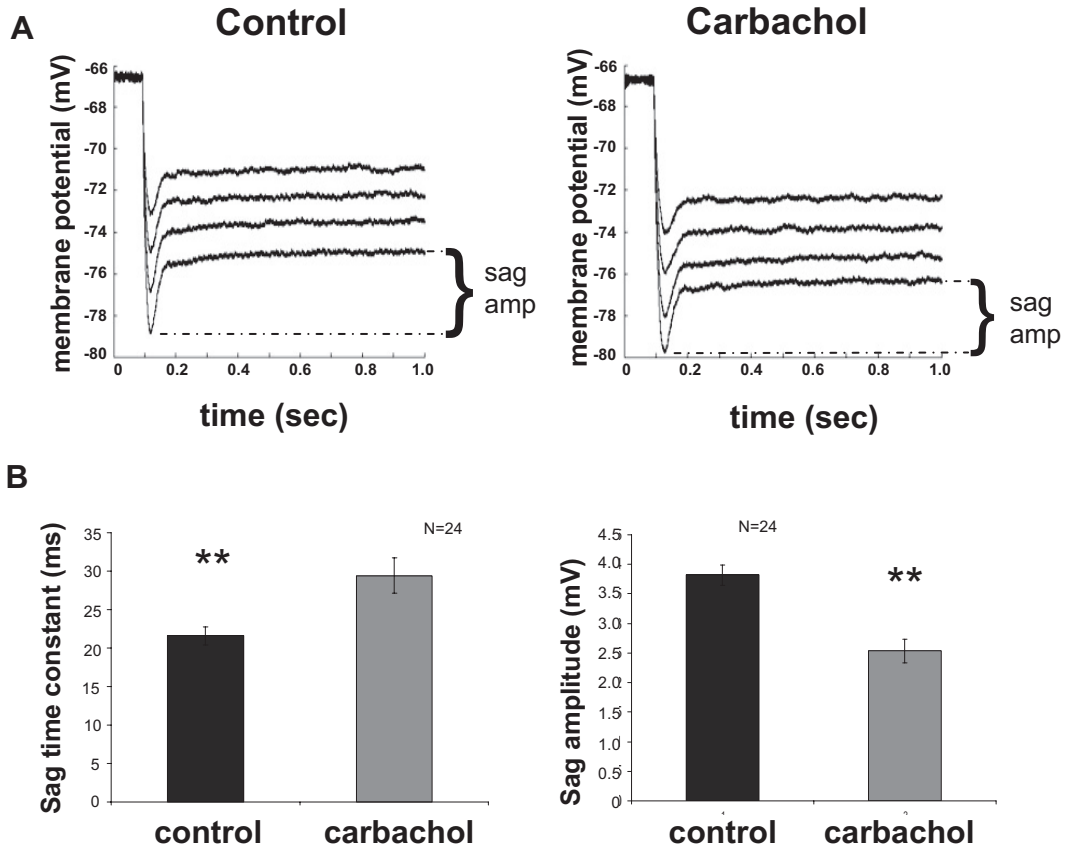

FIG. 5. Analysis of membrane potential sag response suggests mAChR-dependent modulation of h-current. *A*: to measure the membrane potential sag response, SCs were hyperpolarized from −65 mV by injecting −200 to −300 pA current for 3 s. Responses were measured in control conditions (*left*) and after 10 min bath application of 10 μM carbachol solution (*right*). The sag amplitude is measured as the difference between the initial hyperpolarized membrane potential and the steady-state membrane potential. The response was fit with a dual exponential to measure time course of sag response. *B*: the averages across all SCs show an increase in the time constant (*left*) and a significant decrease in sag amplitude (*right*) from the control to the carbachol condition.

change from ZD7288 to ZD7288 with carbachol ($P < 0.01$, $n = 24$ and $n = 6$).

To test the model predictions of an m-current influence on resonance, we recorded SCs at more depolarized potentials and again at more hyperpolarized potentials. The resonance properties at each potential were compared in control solution and after 10 min bath application of 10 μM XE991, which is a selective m-current blocker. The results matched the model predictions and data from CA1 pyramidal neurons, showing m-current–generated membrane potential resonance at depolarized, but not hyperpolarized, membrane potentials (Hu et al. 2002). Recordings from an individual cell at −58 and −68 mV are presented in Fig. 7*A*. The impedance profile averaged across all cells shows the effect of blocking m-current influence at −58 mV (Fig. 7*B, left*). This effect was present in eight of nine cells, and the population averages showed that, at −58 mV, the reduction in resonance frequency (−0.79 ± 0.26 Hz; $P < 0.05$, $n = 9$) is statistically significant, yet there is no statistically significant change at −68 mV (−0.25 ± 0.16 Hz; $P > 0.05$, $n = 9$; Fig. 7*C*). Similarly, the decrease in resonance strength was −0.379 ± 0.100 ($P < 0.01$, $n = 9$) at −58 mV, and the change in resonance strength at −68 mV was 0.029 ± 0.077 ($P < 0.01$, $n = 9$). The resonance strength and resonance frequency have statistically different mean values at −58 versus −68 mV ($P < 0.01$, $n = 9$; Fig. 7*C*).

DISCUSSION

Channel physiology mediates changes in resonance

The results from this study showed that membrane potential resonance can be altered as a function of cholinergic neuromodulation. In particular, activation of mAChRs produces changes in h-current and m-current, both of which shift the resonance frequency and resonance strength to significantly lower values.

Our simulation results suggest that changes in the physiology of several different ion channels could account for the observed changes in resonance frequency and resonance strength. Through co-expression of M1 acetylcholine receptors and H channels comprised of HCN1 and HCN2 subunits in *Xenopus* oocytes, Pian and colleagues showed that the activation of functional mAChRs leads to an increase in the h-current time constant. Furthermore, this change was specific to the distribution of the particular type of HCN subunits used to form functional channels. H-channels comprised of exclusively HCN2 protein experienced a twofold slowing of their time constants, whereas the HCN1 channels slowed down by 1.5 times. Results from this study showed that the percent change in resonance frequency increases along the dorsal to ventral axis of mEC. Because the HCN2 subunits are preferentially modulated by mAChR activation, the increasing modulation of resonance fre-

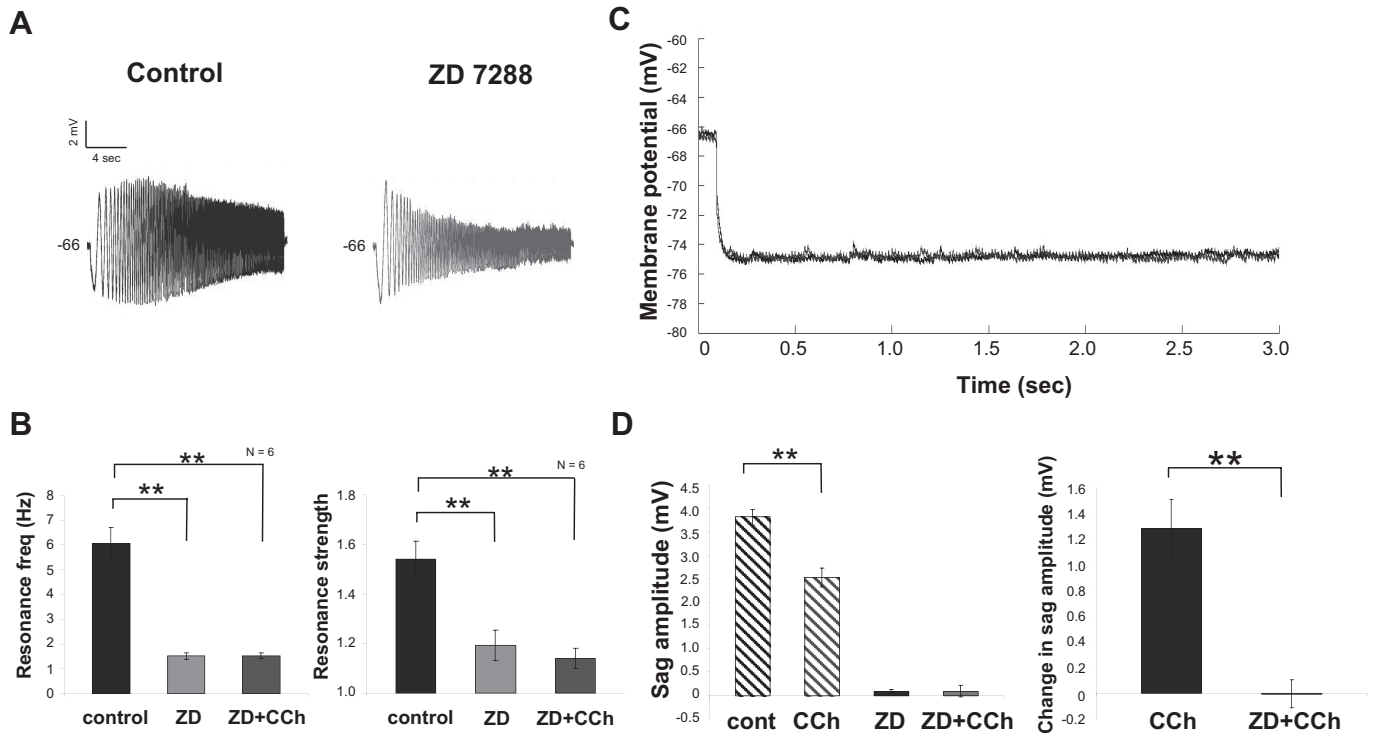

FIG. 6. Pharmacological blockade of cyclic nucleotide-regulated (HCN) channels shows that cholinergic modulation of the resonance properties and the sag response is dependent on the h-current. *A*: ZAP protocols were run in control (*left*) and in the presence of 10 μM ZD7288 (*right*). *B*: resonance frequency was reduced from 6.05 $\pm$ 0.66 Hz in control (black) to 1.52 $\pm$ 0.13 Hz in the ZD7288 (gray) ($P < 0.01$, $n = 6$). Resonance strength was reduced from 1.54 $\pm$ 0.07 in control (black) to 1.19 $\pm$ 0.06 in ZD7288 (gray) ($P < 0.01$, $n = 6$). Addition of carbachol to ZD7288 (red) gave a resonance frequency 1.52 $\pm$ 0.12 Hz and a resonance strength of 1.14 $\pm$ 0.04. *C*: the voltage response caused by hyperpolarizing current steps is shown in 10 μM ZD7288 (black) and in 10 μM ZD7288 with 10 μM carbachol (gray). *D*: blockade of H-channels reduced the sag amplitude to 0.084 $\pm$ 0.034 mV (black, solid), and subsequent application of carbachol had no significant effect on the sag amplitude (0.088 $\pm$ 0.12 mV; gray solid). The change in sag amplitude from control ACSF to carbachol was 1.29 $\pm$ 0.22 mV, and this was significantly different from the change from ZD 7288 to ZD7288 with carbachol (-0.004 ± 0.11 mV; $P < 0.01$, $n = 6$; *D*, *right*).

quency could be explained through a differential HCN subunit composition along this dorsal-ventral axis. Specifically, there could be higher proportion of HCN2 in the ventral region and higher proportion of HCN1 in the dorsal region. In addition, the results from Pian et al. (2007) did not show a change in the h-current–dependent tail current after mAChR activation, suggesting that our observed decrease in sag potential amplitude could be occurring through a separate mechanism from that mediating the change in the sag time constant.

Using pharmacological manipulations, Pian et al. suggested that the interaction between the mAChR and the H-channel is mediated through changes in levels of phosphatidylinositol 4,5-biphosphate. In contrast to the canonical description of PLC-dependent hydrolysis of PIP_2, Pian et al. proposed that increases in PIP_2 caused by PKC-activated synthesis produced the slowing effect in the h-current. Using this framework, further studies may be conducted to assess whether this molecular pathway also modulates h-current in mammalian neurons.

Activation of mAChRs produces an increase in membrane resistance (Cole and Nicoll 1984). It has been suggested by Garden et al. (2008) that a difference in leak conductance along the dorsal to ventral axis of mEC could account for changes in the temporal integration window along this axis. Continuing along this line of evidence, it may seem plausible that a gradient in the maximum leak conductance along the dorsal to ventral axis of mEC could account for the differential dorsal to ventral changes seen in resonance properties. However, recordings from mEC SCs using dynamic clamp (Fernandez and White 2008), and our simulation results showed that changes in resonance frequency depend very weakly on the leak conductance. Furthermore, our model showed that decreasing leak conductance increases resonance strength, which does not agree with our experimental findings on carbachol effects and suggests that mAChR-mediated modulation of passive leak conductance does not account for the observed changes in resonance frequency or resonance strength.

Functional significance of cholinergic modulation of resonance properties

Although h-current and m-current have been shown to both modulate resonance frequency and resonance strength in similar directions as a function of mAChR activation, it remains an open question as to what is the function of this modulation of channel physiology. Given that each current endows the membrane with a similar frequency response, a reasonable possibility is that the neuron uses both currents to tune the cells impedance curve over a larger range of membrane potentials than could be covered with only one of these channels. Both channel resonances are found in CA1 pyramidal neurons in the hippocampus, and it seems plausible that this could be a general feature among many principal cell types in the parahippocampal region (Hu et al. 2002).

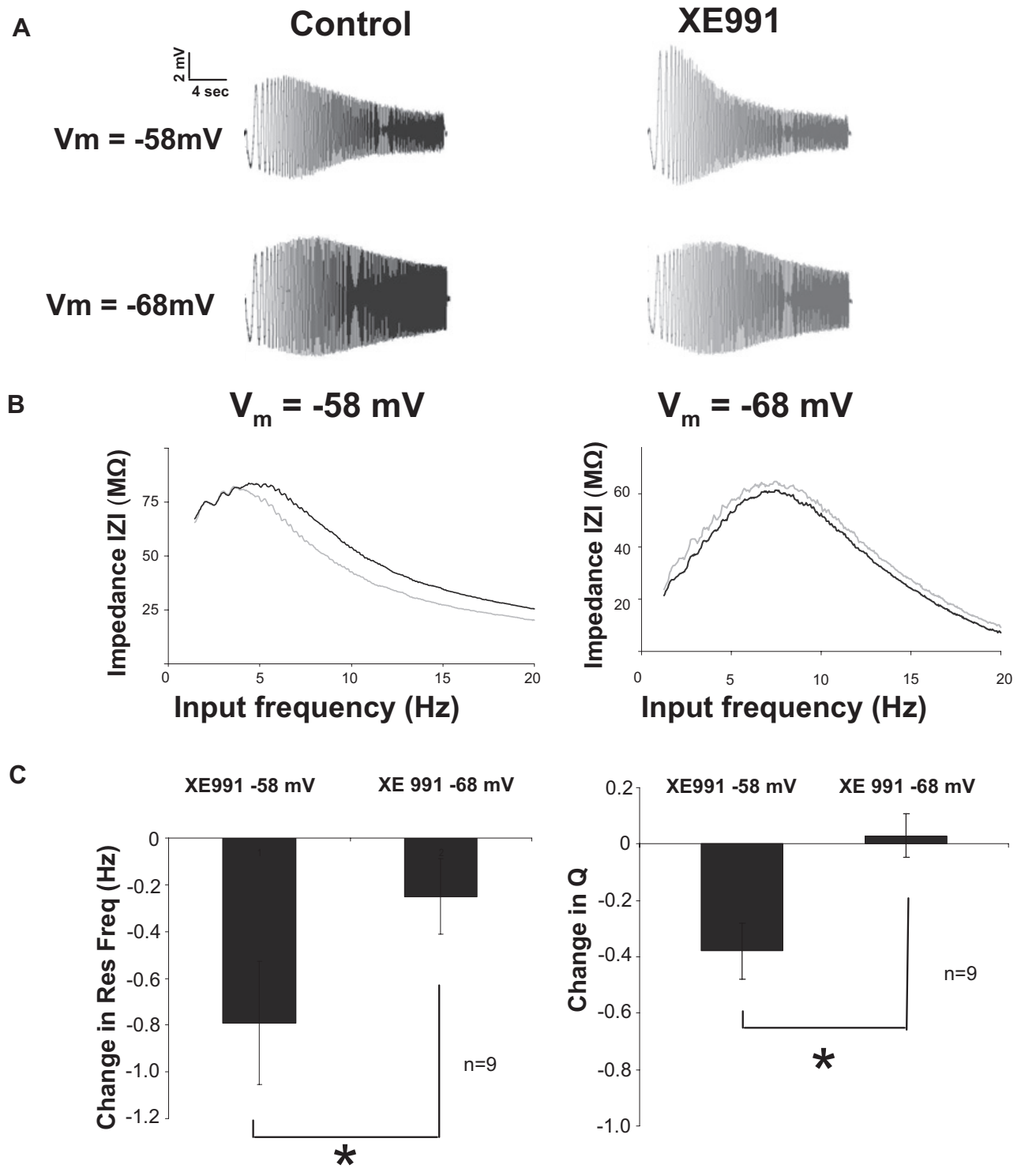

FIG. 7. Pharmacological manipulation of KCNQ channels shows a significant m-current–dependent resonance at depolarized membrane potentials. *A*: individual ZAP responses are shown at −58 mV in control (black) and after 10 min bath application of 10 μM XE991 and again at −68 mV for both conditions. *B*: the plot of the impedance profile depicts the response of the SCs in the control (black) and in the XE991 condition (gray) at the more depolarized membrane potentials of −58 mV (*left*) and at the more hyperpolarized membrane potentials of −68 mV (*right*). *C*: population averages show that the block of m-current decreases resonance frequency from control to XE991 condition at a membrane potential of −58 mV ($P < 0.05$). In contrast, resonance frequency at −68 mV membrane potentials does not show changes that are significantly different from 0. Resonance strength decreases at −58 mV and does not change significantly at −68 mV.

A characteristic feature in the spike train of SCs is the appearance of spike clustering (Alonso and Klink 1993). Spike clustering is captured through inspection of the SCs bimodal interspike interval distribution, and it has been shown that the second peak in the distribution is the result of the SC resonance properties (Engel et al. 2008). The bimodal distribution of the resonant SCs contrasts with the monomodal distribution of the nonresonant layer II mEC pyramidal neurons. The presence of subthreshold membrane potential resonance can be used to distinguish the spiking behavior of resonant and nonresonant neurons. The results of our study suggest that neuromodulation of resonance properties could be used to differentiate spiking behavior of resonant cells across multiple neuromodulatory states.

As described in the Introduction, the spatial periodicity of grid cells (Hafting et al. 2005) and the resonance frequency differ systematically along the dorsal to ventral axis of mEC (Giocomo et al. 2007). A model of grid cells based on oscillatory interference (Burgess 2008; Burgess et al. 2007; Giocomo et al. 2007; Hasselmo 2008) indicated how frequency differences could underlie the grid cell firing pattern, Experimental data showed that grid field spacing (Barry et al. 2009) and levels of acetylcholine in the cortex increase as a function of the novelty of an environment (Acquas et al. 1996; Parikh et al. 2007). The results from this study connect these data by showing that resonance frequency changes as a function of cholinergic modulation. The results from Acquas et al. (1996) and Parikh et al. (2007) suggested that cortical ACh levels increase as an animal explores a novel environment. The data presented in our study lead directly to the prediction that changes in grid cell spacing, induced by exposure to a novel environment, result from changes in ACh levels in mEC and may be caused by changes in the impedance profile of SCs.

ACKNOWLEDGMENTS

We thank C. Andrews, A. Bogaard, and E. Zilli for programming assistance and M. Brandon, E. Newman, and M. Yoshida for helpful comments on earlier manuscripts.

GRANTS

This work was supported by National Institutes of Mental Health Grants R01 MH-61492 and R01 MH-60013, National Science Foundation Sciences of Learning Center CELEST SBE 0354378, and Silvio O. Conte Center Grant MH-71702.

DISCLOSURES

No conflicts of interest, financial or otherwise, are declared by the author(s).

REFERENCES

Acquas E, Wilson C, Fibiger HC. Conditioned and unconditioned stimuli increase frontal cortical and hippocampal acetylcholine release: effects of novelty, habituation, and fear. *J Neurosci* 16: 3089–3096, 1996.

Alonso AA, Klink R. Differential electroresponsiveness of stellate and pyramidal-like cells of medial entorhinal cortex layer II. *J Neurophysiol* 70: 128–143, 1993.

Alonso AA, Llinas RR. Subthreshold Na^+-dependent theta-like rhythmicity in stellate cells of entorhinal cortex layer II. *Nature* 342: 175–177, 1989.

Barry C, Hayman R, Burgess N, Jeffery KJ. Experience-dependent rescaling of entorhinal grids. *Nat Neurosci* 10: 682–684, 2007.

Barry C, O'Keefe J, Burgess N. Effect of novelty on grid cell firing. *Soc Neurosci Abstr* 35: 101.24, 2009.

Burgess N. Grid cells and theta as oscillatory interference: theory and predictions. *Hippocampus* 18: 1157–1174, 2008.

Burgess N, Barry C, O'Keefe J. An oscillatory model of grid cell firing. *Hippocampus* 17: 801–812, 2007.

Cole AE, Nicoll RA. The pharmacology of cholinergic excitatory responses in hippocampal pyramidal cells. *Brain Res* 305: 283–290, 1984.

Destexhe A, Rudolph M, Fellous JM, Sejnowski TJ. Fluctuating synaptic conductances recreate in vivo-like activity in neocortical neurons. *Neuroscience* 107: 13–24, 2001.

Dickson C, Magistretti J, Shalinsky MH, Fransen E, Hasselmo ME, Alonso AA. Properties and role of I_h in pacing of subthreshold oscillations in entorhinal cortex layer II neurons. *J Neurophysiol* 83: 2562–2579, 2000.

Dudman JT, Nolan MF. Stochastically gating ion channels enable patterned spike firing through activity-dependent modulation of spike probability. *PLOS Comp Biol* 5: e1000290, 2009.

Engel TA, Schimansky-Geier L, Herz AVM, Schreiber S, Erchova I. Subthreshold membrane-potential resonances shape spike-train patterns in the entorhinal cortex. *J Neurophysiol* 100: 1576–1589, 2008.

Erchova I, Kreck G, Heinemann U, Herz AVM. Dynamics of rat entorhinal cortex layer II and III cells: characteristics of membrane potential resonance at rest predict oscillation properties near threshold. *J Physiol* 1: 89–110, 2004.

Fernandez FR, White JA. Artificial synaptic conductances reduce subthreshold oscillations and periodic firing in stellate cells of the entorhinal cortex. *J Neurosci* 28: 3790–3803, 2008.

Fransen E, Alonso AA, Dickson CT, Magistretti J, Hasselmo ME. Ionic mechanisms in the generation of subthreshold oscillations and action potential clustering in entorhinal layer II stellate neurons. *Hippocampus* 14: 368–384, 2004.

Fyhn M, Molden S, Witter MP, Moser EI, Moser MB. Spatial representation in the entorhinal cortex. *Science* 305: 1258–1264, 2004.

Garden DLF, Dodson PD, O'Donnell CO, White MD, Nolan MF. Tuning of synaptic integration in the medial entorhinal cortex of the organization of grid cell firing fields. *Neuron* 60: 875–889, 2008.

Gimbarzevsky B, Miura RM, Puil E. Impedance profiles of peripheral and central neurons. *Can J Physiol Pharmacol* 62: 460–462, 1984.

Giocomo LM, Hasselmo ME. Time constants of h current in layer II stellate cells differ along the dorsal to ventral axis of medial entorhinal cortex. *J Neurosci* 28: 9414–9425, 2008.

Giocomo LM, Hasselmo ME. Knock-out of HCN1 subunit flattens dorsal-ventral frequency gradient of medial entorhinal neurons in adult mice. *J Neurosci* 29: 7625–7630, 2009.

Giocomo LM, Zilli EA, Fransen E, Hasselmo ME. Temporal frequency of subthreshold oscillations scales with entorhinal grid cell field spacing. *Science* 315: 1719–1722, 2007.

Haas JS, Dorval AD, White JA. Contributions of Ih to feature selectivity in layer II stellate cells in entorhinal cortex. *J Comp Neurosci* 22: 161–171, 2002.

Hafting T, Fyhn M, Molden S, Moser MB, Moser EI. Microstructure of a spatial map in the entorhinal cortex. *Nature* 436: 801–806, 2005.

Hasselmo ME. Grid cell mechanisms and function: contributions of entorhinal persistent spiking and phase resetting. *Hippocampus* 18: 1213–1229, 2008.

Heys JG, Gicomo LM, Hasselmo ME. A biophysical model shows that h current time constant differences in rat medial entorhinal cortex could underlie differences in membrane potential oscillation frequency. *Soc Neurosci Abstr* 34: 94.17, 2008.

Hu H, Vervaeke K, Storm JF. Two forms of electrical resonance at theta frequencies, generated by M-current, h-current and persistent Na^+ current in rat hippocampal pyramidal cells. *J Physiol* 3: 783–805, 2002.

Hutcheon B, Miura RM, Puil E. Subthreshold resonance in neocortical neurons. *J Neurophysiol* 76: 216–222, 1996.

Hutcheon B, Yarom Y. Resonance, oscillation and the intrinsic frequency preferences of neurons. *Trends Neurosci* 23: 216–222, 2000.

Klink R, Alonso A. Muscarinic modulation of the oscillatory and repetitive firing properties of entorhinal cortex layer II neurons. *J Neurophysiol* 77: 1813–1828, 1997.

Klink R, Alonso A. Ionic mechanisms of muscarinic depolarization in entorhinal cortex layer II neurons. *J Neurophysiol* 77: 1829–1843, 1997a.

Klink R, Alonso A. Morphological characteristics of layer II projection neurons in the rat medial entorhinal cortex. *Hippocampus* 7: 571–583, 1997b.

Lampl I, Yarom Y. Subthreshold oscillations and resonant behavior: two manifestations of the same mechanism. *Neuroscience* 78: 325–341, 1997.

Magistretti J, Alonso A. Biophysical properties and slow voltage-dependent inactivation of a sustained sodium current in entorhinal cortex layer-II principal neurons: a whole-cell and single-channel study. *J Gen Physiol* 114: 491–509, 1999.

Migliore M, Cook E, Jaffe DB, Turner DA, Johnston D. Computer simulations of morphologically reconstructed CA3 hippocampal neurons. *J Neurophysiol* 73: 1157–1168, 1995.

Moser EI, Moser MB. A metric for space. *Hippocampus* 18: 1142–1156, 2008.

Neher E. Correction for liquid junction potential in patch clamp experiments. *Methods Enzymol* 207: 123–131, 1992.

Nolan MF, Dudman JT, Dodson PD, Santoro B. HCN1 channels control resting and active integrative properties of stellate cells from layer II of the entorhinal cortex. *J Neurosci* 27: 12440–12451, 2007.

Parikh V, Kozak R, Martinez V, Sarter M. Prefrontal acetylcholine release controls cue detection on multiple timescales. *Neuron* 56: 141–154, 2007.

Paxinos G, Watson C. The Rat Brain in Stereotaxic Coordinates. New York: Academic, 1998.

Pian P, Bucchi A, DeCostanzo A, Robinson RB, Siegelbaum SA. Modulation of cyclic nucleotide-regulated HCN channels by PIP_2 and receptors coupled to phospholipase C. *Eur J Physiol* 125: 145, 2007.

Pian P, Bucchi A, Robinson RB, Siegelbaum SA. Regulation of gating and rundown of HCN hyperpolarization –activated channels by exogenous and endogenous PIP_2. *J Gen Physiol* 128: 593–604, 2006.

Sargolini F, Fyhn M, Hafting T, McNaughton BL, Witter MP, Moser MB, Moser EI. Conjunctive representation of position, direction and velocity in entorhinal cortex. *Science* 312: 758–762, 2006.

White JA, Klink R, Alonso AA, Kay AR. Noise from voltage-gated ion channels may influence neuronal dynamics in the entorhinal cortex. *J Neurophysiol* 80: 262–269, 1998.

White JA, Rubinstein JT, Kay AR. Channel noise in neurons. *Trends Neurosci* 23: 131–137, 2000.

Yoshida M, Alonso A. ell-type-specific modulation of intrinsic firing properties and subthreshold membrane oscillations by the M(Kv7)-current in neurons of the entorhinal cortex. *J Neurophysiol* 98: 2779–2794, 2007.